Experimental research on self-amplifying density waves in horizontal pipelines of two phase granular slurries

Measurements on the effect of particle diameter and concentration

de Hoog, Edwin; van der Ven, Oscar; Helmons, Rudy; Talmon, Arno; van Rhee, Cees

DOI
10.1016/j.ijmultiphaseflow.2024.105027

Publication date
2024

Document Version
Final published version

Published in
International Journal of Multiphase Flow

Citation (APA)
de Hoog, E., van der Ven, O., Helmons, R., Talmon, A., & van Rhee, C. (2024). Experimental research on self-amplifying density waves in horizontal pipelines of two phase granular slurries: Measurements on the effect of particle diameter and concentration. *International Journal of Multiphase Flow*, *181*, Article 105027. https://doi.org/10.1016/j.ijmultiphaseflow.2024.105027

International Journal of Multiphase Flow 181 (2024) 105027

Contents lists available at ScienceDirect

International Journal of Multiphase Flow

journal homepage: www.elsevier.com/locate/ijmulflow

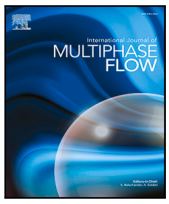

Experimental research on self-amplifying density waves in horizontal pipelines of two phase granular slurries: Measurements on the effect of particle diameter and concentration

Edwin de Hoog [a,b,*], Oscar van der Ven [b], Rudy Helmons [b], Arno Talmon [b,c], Cees van Rhee [b]

[a] Royal IHC, Smitweg 6, Kinderdijk, 2961 AW, The Netherlands
[b] Department of Dredging Engineering, Faculty of Mechanical Engineering, Delft University of Technology, Mekelweg 2, 2628 CD, Delft, The Netherlands
[c] Deltares, Boussinesqweg 1, 2629 HV, Delft, The Netherlands

ARTICLE INFO

Keywords:
Hydraulic transport
Slurry transport
Density waves
Transients
Dredging
Deep seamining

ABSTRACT

Self-amplifying density waves in hydraulic transport pipelines is a scarcely researched topic. Density waves are in essence the result of a spatial redistributing effect and clustering of solids in hydraulic transport pipelines. Self-amplifying density waves are very undesirable for practical applications, as these waves increasing the risk of pipeline blockages. The two available experimental studies (Talmon et al., 2007; Matoušek and Krupička, 2013) report conflicting properties of the density waves, such as wave length and wave celerity. This new experimental research aims to shed light on the reported differences, by broadly varying particle size and concentration in a new dedicated experiment. The main highlight of this research is that two separate mechanisms were identified that can cause density waves, and Talmon et al. (2007) and Matoušek and Krupička (2013) in hindsight were studying the two different mechanism respectively. Both wave type mechanisms come into effect at mixture velocities close to the deposit limit velocity, and require a stationary bed layer to initiate. The first mechanism is caused by an imbalance of erosion and sedimentation of the bed layer, which is predominant for fine sand particles (~242 μm and ~308 μm in this research). The second mechanism occurs when the bed layer starts sliding, instead of being eroded, and is specific for larger sand sizes (~617 μm and ~1.08 mm in this research). These two mechanisms are clearly distinguishable, having different wave lengths, celerity, amplitudes and amplification rates. The results also show a clear relationship between the mean concentration of a density wave, the wave amplitude and wave celerity specific for each of the two mechanisms.

1. Introduction

Hydraulic transportation is the main technology used to transport sediment in many industries like dredging, mining and deep sea mining. Pipelines can be many kilometers long and in case of coarse sediments, centrifugal pumps are often the preferred pump type to drive the system (Visintainer et al., 2023). Flow assurance studies for these pipelines apply steady-state methodologies and mainly involve comparing the operating velocity of the pipeline with a minimum threshold velocity to avoid stationary sediment deposits in the pipeline. This threshold velocity is generally called the deposit limit velocity among academics and engineers.

Even though pipeline designers utilize steady-state methods, the slurry flow in the pipeline is by its nature unsteady. Fluctuations of the mixture velocity are caused by temporal variations in mixture density entering the pipeline through three mechanisms. Firstly, by the unsteady nature of feeding the pipeline, especially in the dredging industry (i.e. the stepping and swaying of a cutter suction dredger). Secondly, by fluctuations in energy losses in the pipeline. Thirdly, due to pump pressure variations, caused by an unsteady mixture density flowing through the centrifugal pump(s). Under the right conditions the aforementioned transients can lead to the spatial redistribution of sediment within the pipeline. In other words, solid particles can agglomerate into density waves, which self-amplify once formed (Matoušek, 1996; Talmon et al., 2007; de Hoog et al., 2021).

Horizontal long distance pipelines can be many kilometers long. When transporting settling slurries, which show a significant non-uniform solids concentration profile over the pipe cross-section, these pipelines are typically designed at a volumetric solids concentration not exceeding 0.15. This upper limit is purely based on field experience in the dredging industry (van den Berg, 2013). Higher concentrations are

* Corresponding author at: Department of Dredging Engineering, Faculty of Mechanical Engineering, Delft University of Technology, Mekelweg 2, 2628 CD, Delft, The Netherlands.
E-mail address: e.dehoog@royalihc.com (E. de Hoog).

https://doi.org/10.1016/j.ijmultiphaseflow.2024.105027
Received 1 November 2023; Received in revised form 2 September 2024; Accepted 11 October 2024
Available online 19 October 2024

Nomenclature

ρ_s	Solids density [kg/m^3].
c	Volumetric concentration [–].
c_{loop}	Average sediments volumetric concentration in the flow loop [–].
c_{mean}	Average concentration measured during density waves in an experiment[–].
c_{nb}	Near bed concentration of solids [–].
c_{vd}	Delivered volumetric concentration [–].
$c_{w,mean}$	Mean concentration of a waves [–].
$c_{w,min}$	Average minimum wave concentration[–].
$c_{w,peak}$	Average wave peak concentration[–].
D	Inner pipe diameter [m].
d_{50}	The median of the particle size distribution [m].
E	Erosion flux [kg/m^2/s].
L_w	Average wave length of the waves [m].
L'_w	Average wave length, corrected for the reduced cross-section above the bed layer [m].
n	Richardson and Zaki exponent [–].
n_0	Bed layer porosity [–].
Q_m	Volumetric flow rate of the mixture [kg/m^3].
Q_s	Volumetric flow rate of solids [kg/m^3].
S	Sedimentation flux [kg/m^2/s].
T_w	Wave period [s].
$u_{m,0}$	The initial mixture velocity of an experiment [m/s].
$u_{m,w}$	The average mixture velocity measured in the presence of density waves [m/s].
u'_w	Average wave celerity, corrected for the reduced cross-section above the bed layer [m/s].
v_{ts}	Terminal settling velocity of a particle [m/s].
y_b	Average bed height [m].

avoided out of fear of density waves and blockages. While in shorter pipelines, for instance found onboard of dredge vessels, volumetric concentrations easily reach 0.35 without any issues. Therefore, much can still be gained in longer pipelines, since the most efficient transport process in terms of energy consumption is at the highest possible concentration, while transporting at the lowest possible mixture velocity. Additionally, increasing concentration will make the transport process more energy efficient and shorten the duration of projects, which constitutes as a gain in cost efficiency. Thus, a better understanding of how self-amplifying density waves form, potentially enables transportation at high concentrations in long pipelines and leads to a more optimized transport process.

The first publicly reported case of self-amplifying density waves was by Matoušek (1996). These waves were ~700 m long at peak concentrations over 0.30 by volume. The pipeline was 10 km long and 650 mm in diameter. Due to the long wave length and high peak concentrations, the waves seriously impeded the safety of the pipeline, and the pump drives had difficulties coping with the strong density waves. The pipeline transported sand with a particle size ranging from fine to medium sand (the average particle size varied in the range of 100–300 μm) with a wide particle size distribution (with 0.07 of the volume larger than 700 μm). The pipeline was used to construct the Prins Clausplein highway junction in The Hague, the Netherlands, and will be referred as such in the remainder of the article. Matoušek (1996) was the first to publish research on these density waves. During this research Matoušek (1996) discovered that the particle velocity is a function of the local particle concentration, being higher at high concentration, and related this physical phenomenon to the development of density waves. However, now it is understood that this variable particle velocity is not the mechanism behind density wave development (Talmon, 1999; de Hoog et al., 2021).

Talmon (1999) developed a theory to explain the Prins Clausplein pipeline density waves, and attributed the wave formation mechanism to an adverse relationship between erosion and sedimentation of the bed layer, using a linear perturbation analysis. This mechanism is referred to as the erosion and sedimentation imbalance, which entails that high concentration flows erode stationary particle deposits, and low concentrations create deposits (at velocities around the deposit limit velocity). As a consequence, local high concentrations cause erosion of the deposit layers. The eroded sediment is transferred to the turbulent suspensions, increasing the local concentration more and flows farther down the pipeline. This increased concentration causes even more erosion in the next pipe section, a continuous cycle that allows the wave to self-amplify. Talmon et al. (2007) dedicated experiments to support the developed theory, and noted that within a closed circular laboratory flow loop a single wave forms with the same length as the flow loop.

Matoušek and Krupička (2013) did experimental research on various unsteady processes in a laboratory flow loop, including density waves. The flow loop had an internal diameter of 100 mm and tests were conducted with 530 μm glass beads. It was observed that at low concentration the regime transition from flow with a stationary bed to flow with a sliding bed was smooth. In contrary, at high concentrations the transition was observed to be unstable. Specifically, at high concentration the bed layer had a shocking sliding behavior, intermittently stationary and mobile, referred to by Matoušek and Krupička (2013) an “unstable slip point” of the bed. Note, Matoušek and Krupička (2013) did not mention what is considered a low and a high concentration. The most important observation by Matoušek and Krupička (2013) was that the development of density waves is associated with the occurrence of the shocking sliding bed behavior, but does not explain how exactly the waves are formed. Additionally, multiple waves were detected in the flow loop, therefore the wave length of these waves was shorter than the flow loop, which is in contradiction with the experimental findings by Talmon et al. (2007).

From this research it became clear that Talmon et al. (2007) and Matoušek and Krupička (2013) were looking at two separate density wave mechanisms (more details in the Theory section). Matoušek and Krupička (2013) mentioned that there was the difference in wave length between the experiments of Talmon et al. (2007) and Matoušek and Krupička (2013) and speculate that "some additional mechanism(s) may contribute to generation of waves", and do not go into further detail on these possible mechanisms. The experiments in this research clearly show the same distinctions in wave length and shows that the density waves are linked to the transport regime. The waves measured by Talmon et al. (2007) were caused by the erosion-sedimentation imbalance, which we call "erosion driven density waves”. While the waves encountered by Matoušek and Krupička (2013) are formed by a different mechanism, which we choose to call “sliding bed driven density waves”, since these waves are in fact sliding bed layers which amplify by absorbing stationary beds. In the Theory section these mechanisms are explained further.

No dedicated study on the effect of the particle diameter on density waves has ever been conducted. In addition, the conflicting reports on the wave lengths between Talmon et al. (2007) and Matoušek and Krupička (2013) was one of the motivations for this experimental research. Therefore, the original research question for these experiments

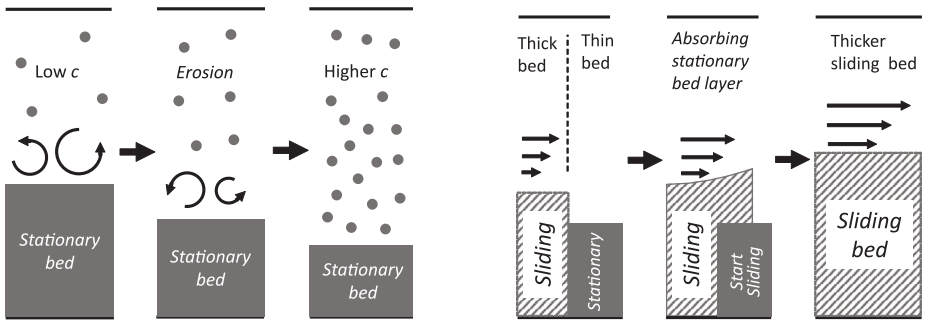

(a) Erosion driven density waves. (b) Sliding bed driven density waves.

Fig. 1. An illustrative representation of the two density wave amplification mechanisms.

was: What is the influence of particle size and concentration on the formation of self-amplifying density waves?

The article starts with a Theory section, explaining the two density wave mechanisms. After which the Methods section elaborates the experimental setup and the techniques used to compute various density wave properties like: mean concentration, peak concentration, wave length and wave celerity. In the Results and Discussion section the measurements are shown and discussed.

2. Theory

The two density wave amplification mechanisms identified in this research are theoretically explained. In support, a graphical explanation is given in Fig. 1.

2.1. Erosion driven density waves

When the mixture velocity exceeds the deposit limit velocity (starting from low velocity) a bed layer of fine sand tends to fully erode and becomes suspended. In terms of flow regime changes we state that the flow regime changes from "stationary bed" to "suspended" mixture flow. This transition is governed by the erosion of the bed layer. The erosion driven density waves are best explained using the mathematical foundation of the theory developed by Talmon (1999). Namely, the erosion and growth of a stationary sediment bed layer can be modeled using an erosion and sedimentation balance (van Rijn, 1984; Winterwerp et al., 1990; van Rhee, 2010; Bisschop, 2018):

$$v_{sed} = \frac{S - E}{\rho_s(1 - n_0 - c_{nb})} \tag{2.1}$$

In Eq. (2.1) v_{sed} is the vertical sedimentation velocity of the bed top interface, S is the sedimentation flux of particles, E the erosion flux, n_0 the bed porosity and c_{nb} the near bed volumetric concentration of particles responsible for the erosion process. When S and E are equal, the bed does not grow or erode. S is often modeled using the established hindered settling approach by Richardson and Zaki (1954):

$$S = \rho_s v_{ts} c_{nb}(1 - c_{nb})^n \tag{2.2}$$

In Eq. (2.2), ρ_s is the particle density, v_{ts} the particle terminal settling velocity and n the particle size dependent Richardson and Zaki (1954) exponent ($2.4 < n < 4.65$). An important property of the settling flux is, that it rises as a function of c_{nb} up-to values of ~0.20 after which it decreases as a function of c_{nb}, see Fig. 2. Meanwhile, the erosion flux E is independent of the concentration for concentrations below ~0.35 (then hindered erosion also plays a role, but this is outside of the scope of this explanation). Moreover, erosion is dictated by inter-particle collisions in a shear layer at the top of the bed layer, which is the typical erosion mode found at high velocities in pipeline flows. Erosion due to shearing is driven by the turbulent kinetic energy of the fluid and does not depend on the concentration (Keetels et al., 2023). Summarized, the sedimentation flux decreases at increasing concentration while erosion remains constant. As a consequence, Eq. (2.1) dictates that at high concentrations (>~0.20), erosion will be dominant. This mechanism allows density waves to self-amplify.

Experimental research by Talmon et al. (2007) aimed to study erosion driven density waves, in a 25 m long, 100 mm diameter flow loop using 200 μm sand. One of the main observations of this experiment was that the density wave which developed was a single wave, with the length equal to the flow loop. Waves were created at volumetric loop concentration from 0.14 to 0.30, but only with a single sand size.

2.2. Sliding bed driven density waves

A stationary bed layer with particles of coarser sand sizes tends to start sliding, instead of fully eroding, when exceeding the deposit limit velocity (starting from a lower velocity). In other words the flow regime changes from a "stationary bed" to a "sliding bed" regime. The exact threshold particle size depends on the pipe diameter, and as an indication it is somewhere between 308–617 μm (based on the experimental results of this research), but is possibly also a function of the grading of the sediment (more in the Results & Discussion section). The regime change threshold is called the deposit limit velocity, and is sensitive to the local cross-section averaged concentration in the pipe.

Modeling of the transition between the stationary bed and sliding bed regimes, can be achieved using steady-state two-layer models (Wilson et al., 2006; Matoušek et al., 2018; Visintainer et al., 2023). These two layer models evaluate a force balance between the hydrodynamic bed shear stress, (which pulls on the bed layer) and the Coulombic friction of the bed layer against the pipe wall (which resist the bed layer from sliding). If the bed shear force exceeds the static friction force the bed layer starts sliding. Local higher cross-section averaged concentrations have thicker bed layers, which experience more bed shear stress. This is caused by the reduced cross-section above the bed, which causes a higher velocity above the bed at equal flow rate, thus increasing the bed shear stress. The bed shear force is a higher order effect than the friction of the bed layer against the pipe wall, thus as a function of increasing bed thickness the bed shear stress increases at a faster rate than the bed friction. As a consequence, thicker beds will slide while thinner beds remain stationary, at equal flow rates. Summarized, a bed layer can slide at local high concentrations, which remains stationary at lower local concentrations.

Fig. 3 shows the deposit limit velocity u_{dl} as a function of the cross-sections average concentration c, computed with a steady-state two-layer model (Wilson et al., 2006). In Fig. 3 we see that for concentrations above ~0.10 bed layers will slide for higher concentrations. Thus a local high concentration can initiate a sliding bed, while other parts of the flow remains stationary.

Once a local high concentration perturbation causes the bed layer to slide the solid particles in the stationary bed layer now become

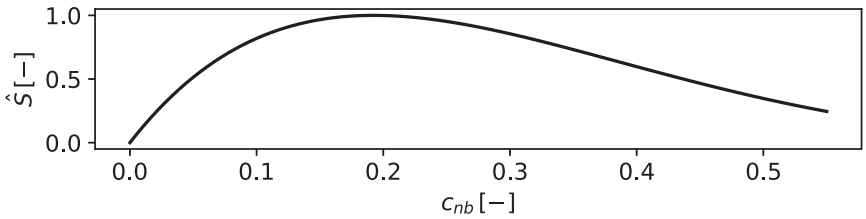

Fig. 2. The hindered effect of the sedimentation flux (Eq. (2.2)) as a function of c_{nb}. $\hat{S} = S/max(S)$.

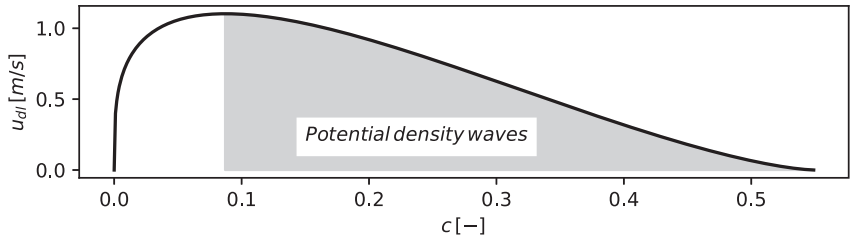

Fig. 3. The deposit limit velocity u_{dl} as a function of the cross-section averaged concentration in the pipe c, computed with the Wilson two layer model (pipe diameter $D = 42$ mm and the particle diameter $d_{50} = 1.08$ mm). If the mean concentration in the pipe is higher than the concentration maximum in the u_{dl} curve, sliding bed driven density waves can be formed if the mixture velocity is close to the deposit limit.

mobile and part of the mixture flow. This was observed with high speed camera footage taken as part of the experiments of this research. As such, the local cross-section averaged transport rate of solids will quickly increases. The density wave flows through the system and the camera footage showed that stationary bed layers start sliding *en-bloc* as the wave flows over the stationary bed layer. Thus quite suddenly the mixture concentration increases once the bed layer mobilizes, which is expressed in the measured data as a sudden rapid amplification of the transport rate of solids (see the Results & Discussion section for more details). This amplification process takes place at the front of the wave. The deposit limit velocity is lower for higher local cross-section averaged concentrations (see Fig. 3), and as such the bed layer will remain mobile once amplified. This local amplified higher concentrated mixture will flow down the pipeline and continue to mobilize stationary bed layers, and amplify to a steady maximum (more details in the Results & Discussion section).

Behind a sliding bed driven density wave two scenarios were observed. (1) The pipeline is momentarily empty and thereafter a new wave appears, or (2) a deposit is restored from particles in the tail of the sliding bed driven density wave.

The empty section can be caused by the sudden sliding of the bed layer at the first moment of initiation of the wave. Consider the local high concentration perturbation from which bed layer started sliding for the first time (through the mechanism as explained in the previous paragraphs). Up-stream of this high concentration perturbation, the bed layer will remain stationary, as the local concentration was not high enough to cause the bed to slide (see Fig. 3). At the location of the high concentration perturbation the bed layer will start sliding *en-bloc*. This will create a zone at the location of the initial local perturbation, where no more bed layer is present, since this bed layer is now sliding now down the pipeline. Like a train leaving the train station, but leaving one of its carts behind. This zone is not filled up again quickly, since the bed layer up-stream of the initial concentration perturbation remained stationary. This creates a gap with very little material, and it was observed to be completely empty of particles on many occasions on the camera footage. Some particles can fill this empty zone, which come from the sheet flow layer flow over the up-stream stationary bed.

The second scenario is that the bed layer can restore behind a bed driven density wave. Moreover, it was observed that the new bed layer grows and restores from particles in the tail of the density wave. Research by Matoušek (1996) and de Hoog et al. (2021) has shown the cross-section averaged particle velocity is higher for higher concentration, experimentally and numerically respectively. Talmon (1999), Talmon et al. (2007) and de Hoog et al. (2021) show how this proportionally causes saw-tooth shaped density waves, a property which has been observed now in many studies on density waves, and has been simulated numerically (de Hoog et al., 2021; de Hoog et al., 2022; de Hoog et al., 2024). This proportionally between the cross-sectional average particle velocity and the concentration results in the fact that the front of a density wave, which has the highest concentration, will always travel fastest of all parts of the wave. This characteristic stretches the wave, with the front of the wave flowing fastest, and the tail the slowest. This in fact causes the saw-tooth shape, and results in a low concentration tail of the wave. This low concentration tail can form a deposit again, if the local deposit limit velocity is higher than the mixture velocity (see Fig. 3). This has been observed in the experiments of this research. However not always, since sometimes the pipe is empty and a new wave passes as explained before. When and why one of the two scenarios occurs, we cannot yet explain.

Summarized, in the view of the authors the inverse proportionally between the deposit limit velocity and the local concentration (at concentrations above ~0.10, see Fig. 3), is the foundational mechanism which triggers the formation of sliding bed driven density waves and is the second mechanism discussed in this article that causes density wave amplification. Since this mechanism is directly related to the sliding bed regime, these waves are called “sliding bed driven” density waves in the remainder of the article.

Fig. 3 also helps explaining one of the main observations by Matoušek and Krupička (2013). Specifically, at low concentration a stable transition towards a sliding bed was observed, and at high concentration the transition was unstable with a sliding and shocking bed layer. Furthermore, density waves were associated with the sliding shocking behavior. The shocking bed behavior is not a fully developed density wave, but a scenario when the bed briefly slides and becomes stationary again. It makes sense that the shocking bed occurs at concentrations above 0.10 according to Fig. 3, since tiny changes in local concentration can cause the bed to slide briefly, and when these local gradients are small enough they will be damped by turbulence and will not grow into large waves. Additionally, in Fig. 3 the deposit limit velocity increases with concentrations below 0.10. Thus, under these conditions instabilities cannot lead to density waves, nor a shocking bed, which explains why the transition to a sliding bed is smooth.

3. Methods

3.1. Experimental setup

To study density waves and the effect of the particle diameter and concentration, a dedicated experimental flow loop was built. The philosophy behind the flow loop design was to build a flow loop with the largest length over pipe diameter ratio as possible, longer than previous experimental research (Talmon et al. (2007): $L/D = 250$, Matoušek and Krupička (2013): $L/D = 520$), within constrains of the laboratory size. The philosophy was to test if the density wave length indeed equals the system length like found in Talmon et al. (2007) and de Hoog et al. (2021), or perhaps a limit to the wave length is possible, which would explain the density waves found in Matoušek and Krupička (2013). A secondary reason for a long flow loop is to avoid damping of the waves. More specifically, axial turbulent dispersion dampens waves and increases with the local longitudinal concentration gradient (Taylor, 1954). In shorter circuits the longitudinal concentration gradient of a wave is higher, assuming the same wave forms and that the wave length equals the system length. As such, shorter circuits have a stronger damping effect on density waves, which can prevent waves from developing. The above design criteria resulted in a flow loop with an inner diameter of 42 mm, and a total length of 45.5 m, which is 1083 pipe diameters. See Fig. 4 for a schematic of the loop.

The loop was built using transparent PVC to be able to visually observe the density waves in the entire flow loop, which is required to detect a sliding bed layer. A 22 kW pump was used to drive the system. Two vertical U-loops were used to measure the delivered concentration c_{vd} at two locations in the loop (Clift and Clift, 1981). Two cameras were used to record the slurry flow between the two U-loops. The delivered concentration is defined as the solids flow rate Q_s over the volumetric mixture flow rate Q_m:

$$c_{vd} = Q_s/Q_m \tag{3.1}$$

Dispersion due to bends was kept to a minimum by using the U-loops and centrifugal pump to make major directional changes, and a long radius bend ($R = 1.5$ m) was used to complete the loop. The mixture velocity was measured using an Electromagnetic Flow Meter (EMF) of type Krohne Optiflux 4000, 0...12 m/s, with an accuracy of ±0.5% full range. The pressure sensors in the U-loop were of the type Druck, Unik 5000, −50...+50 kPa differential pressure transducers with an accuracy of ±0.04% full range. All sensors were calibrated at the start of experimental program. The sensor signals were logged at a sampling rate of 2 kHz using a 24 bit data logger.

Four sieved quartz sand types were used for the experiments. The sand types are Zilverzand (Zz) with a particle diameter of $d_{50} = 242$ µm and Dorsilit types 7, 8 and 9 (D7, D8 and D9 respectively), with particle diameters of $d_{50} = 1.09$ mm, $d_{50} = 617$ µm and $d_{50} = 308$ µm, respectively. These sand types have a very narrow grading, see Fig. 5.

Nineteen tests were conducted with the four sand types by varying the average loop volumetric concentration of solids between 0.10 and 0.25. Each test started by filling the flow loop to a desired concentration, and at high mixture velocity ($\gg u_{dl}$) such that concentration variations could dampen out. After this initial period the pump revolutions, and therefore flow rate, were slowly lowered over a period of several minutes until a bed layer formed. From that point on the pump revolutions were kept constant, and the density waves were allowed to develop. After some time the waves reached a steady-state amplitude, these steady-state periods were used for the data analysis, like determining peak concentration, wave lengths and the celerity. See Fig. 6 for an example of an experiment.

3.2. Computing wave properties

The focus of these experiments was to measure as many density wave related parameters as possible, such as the wave length, celerity, and peak concentration. The measuring principles and algorithms used to extract these properties from the data are explained in this section.

The wave celerity was computed by cross-correlation of the measured time traces of the two U-loops. This results in a time lag between the signals, and with the known distance between the U-loops, the wave celerity could be computed using the cross-correlation. The best results were obtained by first normalizing both measurements. Specifically, the measurements are normalized with respect to their average and maximum concentration value. This results in traces with values between 1 and -1. Without this procedure the correlation is not always successful. Fig. 7 shows an example of the time shift computed using the cross-correlation technique. Fig. 7(a) shows the original U-loop time traces, and 7(b) shows the same traces where U-loop 2 is shifted in time based on results attained using the cross-correlation method, making the signals overlap. From experience of using this algorithm, we deduced that the correlation is highest at the steep upwards gradient at the wave front. The correlation is computed from an entire steady-state section of an experiment which can last several minutes. During this time the waves have recirculated many times, and sometimes develop and merge into new waves. As such, the computed wave celerity represent the average celerity of all waves in the loop, temporally averaged over an experiment.

The wave length is straight forward to measure in case of erosion driven density waves, since these produced a very clear single periodic wave. As such, the wave period is simply computed from the time between peaks of the U-loop c_{vd} measurements, and the wave length is computed as the product of the wave celerity and the wave period. However, in case of sliding bed driven density waves the wave length is not periodic. Multiple waves in a loop were present, and at times they merge into a larger waves with twice the length (see Fig. 8(a)). Therefore, a different approach was taken to measure the wave length of the sliding bed driven density waves.

An three step algorithm was developed to detect the flat sections between the sliding bed driven waves. These flat sections occurred in all experiments with sliding bed driven density waves. The first step was to reduce noise, by passing the time traces through a low pass filter with a cut-off frequency of 2 Hz. Secondly, the derivative of the entire trace was computed. The condition $\frac{\partial c}{\partial t} < 1^{-5}$ was applied to detect the flatter sections, which was chosen by trail and error such that the waves were successfully isolated. Thirdly, a condition was applied to filter out very small low gradient sections of only a few time samples. The shortest flat spot allowed was 1000 samples (=0.5 s), again this value chosen by visually judging that the waves were successfully isolated. With the flat sections isolated, the waves were said to be anything that is not a flat section, see Fig. 8(b). From an isolated wave, the wave period and the wave length could be determined. Applying this method for all waves in a time trace, resulted in a distribution of wave periods (see Fig. 9(a)). From this distribution the average wave period was computed and considered to be the average of the entire experiment. From this average wave period the wave length could be calculated by multiplication with the wave celerity. Note that sometimes the isolation algorithm fails to isolate a wave, for example at 2475 s Fig. 8(b). However, enough wave samples are found in an experiment (samples sizes ranging from 13–167 waves, depending on the experiment) that such irregularities are not frequent enough to significantly influence the final averaged value.

The wave maxima, minima and average concentrations were again straight forward to determine in case of the erosion driven density waves. A peak finding algorithm available in the Python Scipy library was applied to find local maxima and minima in the U-loop time traces (*scipy.signal.find_peaks()*). In case of the sliding bed driven density waves, the wave peak concentration was computed from the maximum

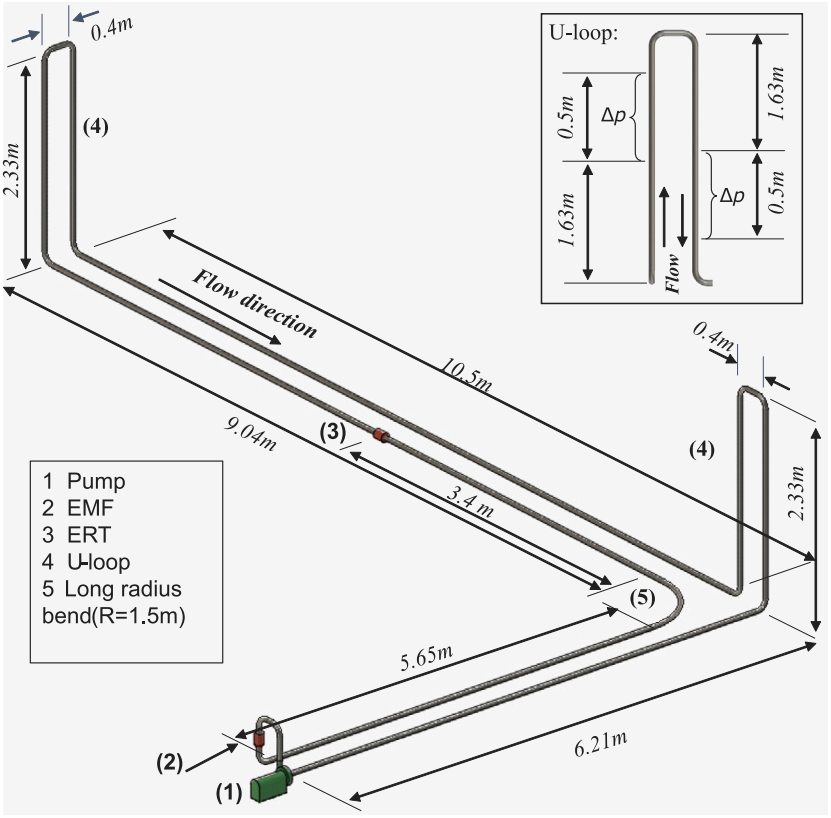

Fig. 4. A schematic of the flow loop, showing sensor locations and dimensions on the pipe segments.

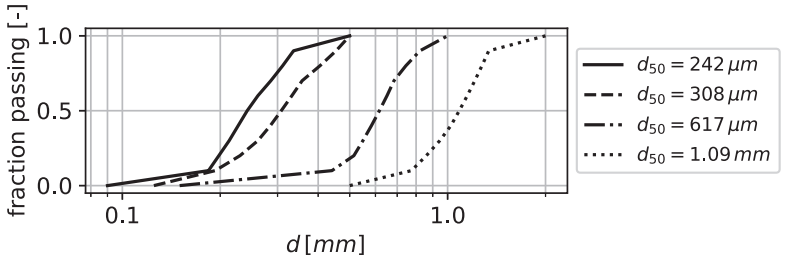

Fig. 5. The particle size distribution of the sand types used for the experiments.

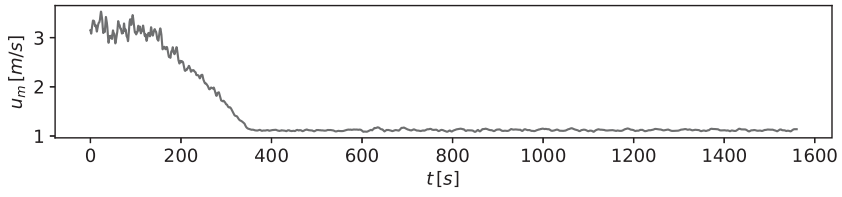

(a) Mixture velocity

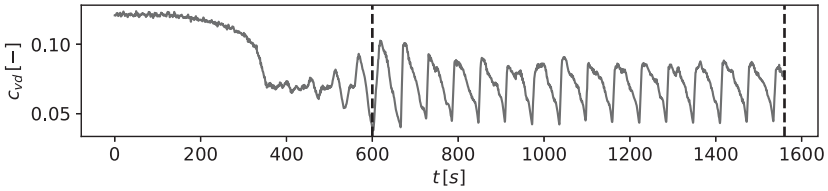

(b) Delivered concentration. The two vertical dashed lines indicates the part used for the data analysis.

Fig. 6. Test Zilverzand (Zz), nr. 1, $d_{50} = 242$ µm. This is an example of erosion driven density waves.

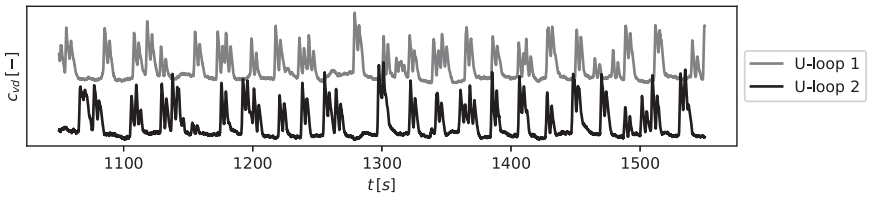

(a) Original time traces.

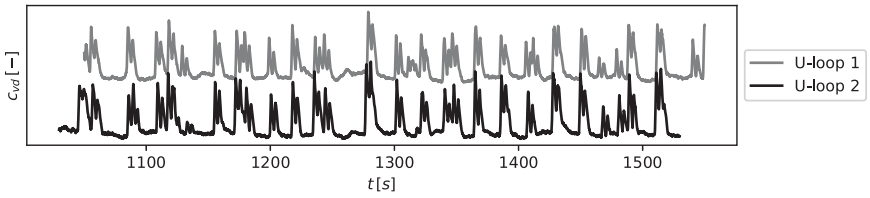

(b) U-loop 2 shifted in time based on the cross-correlation method.

Fig. 7. An example of the cross-correlation technique to measure the velocity of both wave types.

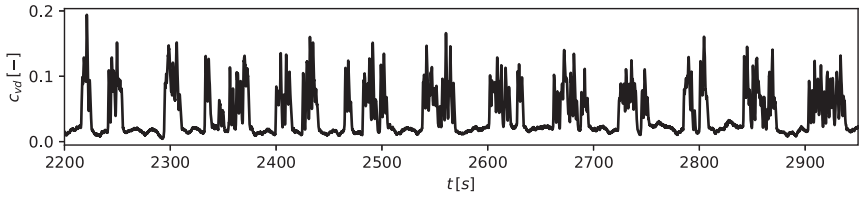

(a) A closer view of sliding bed driven density waves.

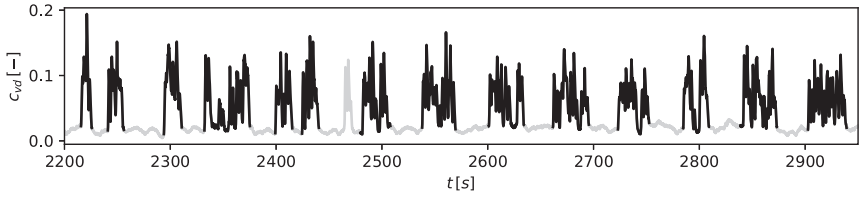

(b) Isolation of the waves using an algorithm that detects the flat sections between the waves.

Fig. 8. An example of sliding bed driven density waves.

from each isolated wave, using the aforementioned wave isolation algorithm. The minima were computed from the minimum of the flat sections in between the sliding bed driven waves. This produced three normal distributions for the maxima, means and the minima of the isolated sliding bed waves (see Figs. 9(b), 9(c), 9(d), respectively). The average of each distribution was taken as the average of the entire time trace.

4. Results & discussion

All properties of the experiments and the density waves can be viewed in Table 1. The time traces of the mixture velocity and delivered concentration of all experiments can be viewed in Fig. 6 and in the Appendix (see Figs. 14–26). Only the delivered concentration of the first U-loop is plotted, to avoid clutter in the graphs. The data analysis section of an experiment is highlighted with two vertical dashed lines in the Figures. Some experiments have two or three sections that were used to analyze the density waves. These are numbered in the graphs, and respectively named in Table 1. The bed height y_b was determined visually from camera footage. This represents an average bed height, since it slightly fluctuates as different concentration parts of a wave passing the camera. Unfortunately, the water during experiment D9, 2.2 and 2.3 was too turbid to observe the bed layer on the camera footage, and therefore are not given in Table 1.

The main highlight of this article is the clear distinction in behavior of the two wave types. The 242 μm and 308 μm sand produced erosion driven density waves. These waves developed relatively slowly, requiring several circulations through the flow loop to reach a steady amplitude. A tiny stationary bed layer was always present at the bottom of the pipe, thus not all sediment was eroded and suspended into the density waves.

The 617 μm and 1.08 mm sand showed sliding bed driven density waves. These waves developed to full amplitude very quickly, usually within one circulation of the loop. These waves were also able to fully

Table 1
All density wave properties that were computed from the experiments.

	d_{50} [mm]	c_{loop} [–]	$u_{m,0}$ [–]	$c_{w,mean}$ [–]	$c_{w,peak}$ [–]	$c_{w,min}$ [–]	c_{mean} [–]	$u_{m,w}$ [m/s]	u_w [m/s]	L_w [m]	$\frac{y_{b,mean}}{D}$ [–]	u'_w [m/s]	L'_w [m]
Zz 1	0.242	0.10	2.94	0.05	0.09	0.04	0.05	1.12	0.79	49.3	0.06	0.77	47.9
Zz 2.1	0.242	0.15	2.07	0.08	0.13	0.06	0.08	1.00	0.82	48.7	0.14	0.75	44.0
Zz 2.2	0.242	0.13	1.54	0.14	0.17	0.08	0.14	1.24	1.09	47.4	0.08	1.04	45.4
Zz 3	0.242	0.18	2.38	0.13	0.18	0.09	0.13	1.17	1.06	47.6	0.11	0.99	44.4
D9 1.1	0.308	0.10	2.31	0.08	0.10	0.03	0.08	1.33	1.08	50.2	0.07	1.04	48.4
D9 1.2	0.308	0.08	1.81	0.05	0.07	0.01	0.05	1.05	0.73	52.0	0.16	0.65	46.0
D9 2.1	0.308	0.16	2.17	0.07	0.09	0.02	0.07	0.84	0.65	50.6	0.11	0.61	47.2
D9 2.2	0.308	0.15	1.93	0.03	0.04	0.01	0.03	0.64	0.40	53.2	n/a	n/a	n/a
D9 2.3	0.308	0.12	1.59	0.01	0.01	0.00	0.01	0.50	n/a	52.8	n/a	n/a	n/a
D8 1	0.617	0.12	3.41	0.06	0.13	0.01	0.05	1.06	1.03	7.2	0.16	0.91	6.3
D8 2	0.617	0.19	3.04	0.06	0.10	0.02	0.04	0.68	0.77	6.3	0.29	0.56	4.6
D8 3	0.617	0.17	1.26	0.15	0.31	0.06	0.12	0.64	0.99	36.8	0.41	0.57	21.0
D8 4	0.617	0.19	1.56	0.14	0.30	0.05	0.12	0.62	0.95	40.9	0.39	0.57	24.4
D7 1	1.08	0.13	3.10	0.07	0.14	0.02	0.05	0.89	0.80	29.4	0.21	0.67	24.3
D7 2	1.08	0.12	2.36	0.07	0.15	0.02	0.05	0.85	0.82	25.4	0.20	0.69	21.4
D7 3	1.08	0.19	2.86	0.10	0.19	0.01	0.07	0.71	0.87	35.3	0.30	0.62	25.3
D7 4	1.08	0.24	1.92	0.13	0.23	0.06	0.12	0.61	0.91	44.1	0.41	0.52	25.1
D7 5	1.08	0.20	1.09	0.13	0.24	0.06	0.12	0.62	0.85	40.6	0.43	0.46	22.0

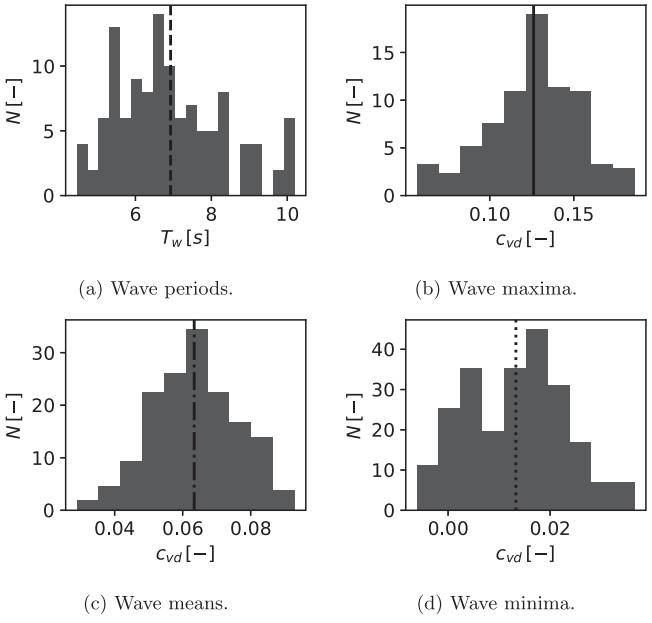

(a) Wave periods. (b) Wave maxima.

(c) Wave means. (d) Wave minima.

Fig. 9. An example experiment, showing the distribution of the wave periods T_w, the concentration maxima, means and minima. The average of the distribution was considered as the average wave length of an experiment.

mobilize the bed, leaving behind sections with only water. This was observed mainly visually and could not be measured well with in the delivered concentration measurements. Furthermore, these zero concentration periods occurred mainly within a wave period as depicted in Fig. 8, and should not be confused with the long flat sections between the waves. The flat sections in Fig. 8 are periods when no wave passes the U-loops and the horizontal section around the U-loops contained a stationary bed layer, which recovered after a wave passed (for more details see the Theory section). The stationary bed layer had a smooth top with a small sheet flow layer which is depicted as a small amount of solids transport in the flat sections of Fig. 8. The zero concentration periods were very short and as such the U-loop could not measure the zero concentration sections well, since the U-loop measurement is based on spatially averaging pressure signals over a distance of 3.03 m. As such, for a zero concentration period to be fully measured, it should be at least be 3.03 m long, which was not often the case.

Some interesting relationships between the density wave parameters (see Table 1) have been discovered. For instance, Fig. 10 shows that the wave peak concentration $c_{w,peak}$ correlates strongly with the average concentration of the wave $c_{w,mean}$, for both wave types. Interestingly, the peak concentration of erosion driven density waves is roughly 1.5 times the average concentration. The data from Talmon et al. (2007) is also plotted in Fig. 10(a), which shows that this trend also continues for erosion driven waves measured in a 100 mm diameter pipe, with mean concentrations up to 0.3. Apparently, the erosion driven wave mechanism shares common properties, which also applies to the larger 100 mm pipes, and is not very sensitive to the particle diameter. However, at this point we do not have an explanation for the $c_{w,peak} \approx 1.5 \cdot c_{w,mean}$ property.

In case of the sliding bed waves the wave peak concentration is twice the average, $c_{w,peak} \approx 2.0 \cdot c_{w,mean}$, as seen in Fig. 10(b). In case of an idealized saw-tooth shaped wave, when the peak of the wave equals twice the average, than minimum should equals zero. This can indeed be the case, as it was observed that empty pipe sections can occur behind a sliding bed driven density wave (more details in the Theory section). Erosion driven density waves do not show empty pipe sections.

The next interesting property is that the wave celerity u_w is a function of the mean wave concentration. In Fig. 11(a) the measured wave celerity over the mixture velocity u_w/u_m is plotted against the mean wave concentration, for both wave types. Interestingly, the sliding bed driven density waves consistently propagate faster than the mixture velocity. It is physically impossible that the particles flow faster than the carrier fluid, therefore another effect must be responsible for the high wave celerity. This phenomena was also mentioned by Matoušek and Krupička (2013). During this research it was noted that the cross-correlation technique used to compute u_w finds its highest correlation at the front of the density waves, since at the front the concentration gradient is highest. As such, u_w measured with the cross-correlation technique can be said to best represent the velocity of the wave front. Furthermore, the front of a wave was observed to flow over a stationary bed layer. Therefore, the reduced cross-section above the sliding bed layer increases the velocity above the bed and therefore also the velocity of the wave front. The reduced cross-section raises the computed wave velocity above the mixture velocity, because the mixture velocity is measured in a vertical pipe, which cannot contain a bed layer. To test this hypothesis, the wave celerity was corrected for the reduced cross-section above the sliding bed layer. The corrected wave celerity

$$u'_w = u_w \frac{A'}{A} \tag{4.1}$$

is computed from the reduced flow area above the stationary bed layer A' just in front of the wave. Fig. 11(b) shows all corrected wave

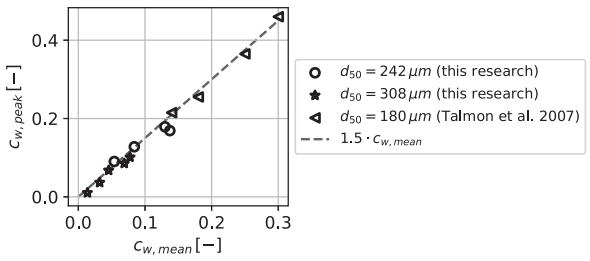

(a) Erosion driven density waves.

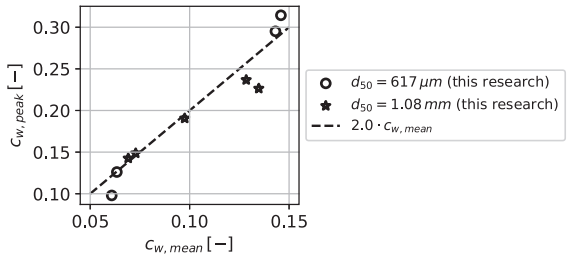

(b) Sliding bed driven density waves.

Fig. 10. The measured wave peak concentration as a function of the wave mean concentration.

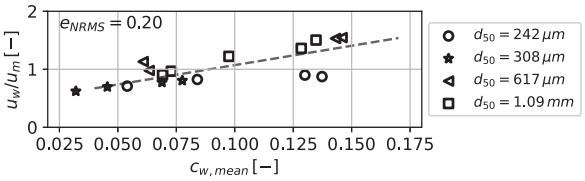

(a) Without correcting for the reduced flow cross-section.

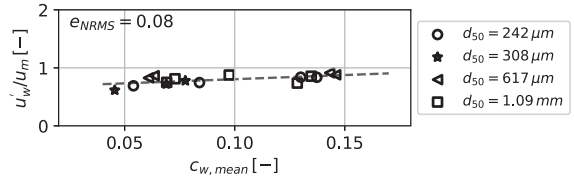

(b) After correction for the reduced flow cross-section.

Fig. 11. The wave celerity as a function of the mean concentration. e_{NRMS} is the normalized root means square error of the fitted linear curve.

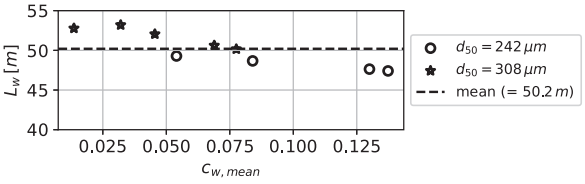

(a) Without correcting for the reduced flow cross-section.

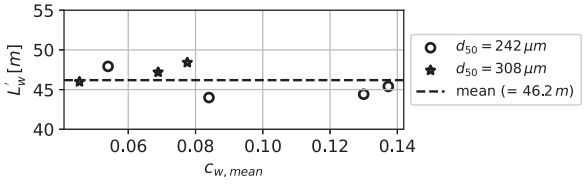

(b) After correction for the reduced flow cross-section.

Fig. 12. The wave lengths of the erosion driven density waves.

celerities u_w' as a function of the mean wave concentration. The corrected wave celerity forms a linear trend, regardless of the wave type. To quantify how good the linear trend is, the normalized-root-mean-square-error e_{NRMS} was computed, which very suitable to compare different data sets, and is zero for a perfect linear fit. The resulting e_{NRMS} is given in Figs. 11(a) and 11(b). By applying the reduced cross-section correction, the e_{NRMS} improved from 0.2 to 0.08, suggesting that the hypothesis of the reduced cross-section is indeed a plausible mechanism which increases the wave celerity above the mixture velocity. The point of this analysis is to understand why the measured wave celerity can be higher than the mixture velocity. From the result we can simply concluded that in case of sliding bed driven, the front of the wave which corresponds with the wave velocity computed with the cross-correlation technique, traveled over a stationary bed during these experiments.

A bed layer is always present in the pipeline in case of erosion bed driven density waves. Yet, the wave celerity u_w does not go above u_m as is the case with the sliding bed driven density waves. The difference can be explained with the thickness of the bed layer. With sliding bed driven density waves the bed layer just in front of the wave is much thicker than the erosion driven density waves. Moreover, the bed thickness during the passing of an erosion driven density waves varies over time. The thinnest bed occurs while the high concentrated wave front passes, since at the front of the wave erosion is higher (see Theory section for more details). Furthermore, the bed layer is the thickest in the tail of the wave, because in the tail the concentration is lowest. In addition, the cross-correlation technique tends to measure the wave velocity at the front of the wave. Summarized, the thickness of the bed at the front of an erosion driven is very thin, thus the effect on reducing the cross-section is very low. As such, the wave celerity does is not increased significantly enough to be higher than u_m. Therefore, the velocity difference between u_w and u_m in case of erosion driven density waves mostly represents the discharge area cross-section averaged slip between the water and the particles.

Another notable property is the measured wave length, given in Fig. 12(a). This shows that the measured wave lengths are consistently above the length of the flow loop (45.5 m), in case of the erosion driven density waves. Naturally this is not possible, since the longest wave that can be contained in the flow loop must have the same length as the loop. This error comes from the fact that the wave length is computed from the wave period, and more importantly, from the wave celerity. As mentioned before, the wave celerity is higher due to the reduced cross-section above the bed. Correcting the wave length from the corrected wave celerity u_w', allows us to compute a corrected wave length L_w', which is plotted in Fig. 12(b). The average value of the corrected wave lengths is 46.2 ±4.2 m, and the loop length now falls within the spread of the data points. The wave length of the sliding bed driven density waves as a function of the mean wave concentration is plotted in Fig. 13. No clear trend can be deduced from this, other than that the 1.08 mm sand produces longer waves than the 617 μm sand. Why sliding bed waves are longer for larger particles is currently still unknown, and is worth investigating in future research.

The new insights on how the wave peak concentration is related to the wave average concentration is very valuable for pipeline designers, assuming these trends are also valid for larger pipeline diameters. This assumption is not far fetched, as the flow regimes dictating the density wave types also occur in larger pipe diameters (i.e.the stationary bed, sliding bed and the suspended flow regimes). The average wave concentration is the same and the mean slurry concentration in case of erosion driven density waves, and 0.01 to 0.02 higher in case of

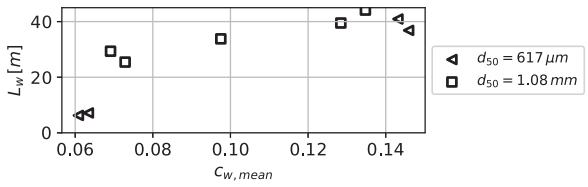

(a) Without correcting for the reduced flow cross-section.

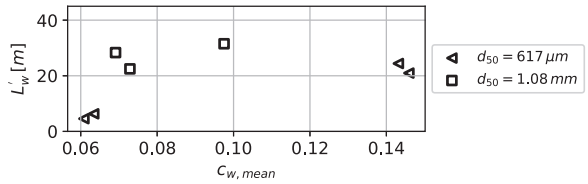

(b) After correction for the reduced flow cross-section.

Fig. 13. The wave lengths of the sliding bed driven density waves.

sliding bed driven density waves. Therefore, as pipeline designer a rough estimation of the wave peak concentration can be made based on the average design concentration of the pipeline.

With this knowledge designers can estimate the amplitude and effect of density waves if waves are expected, for instance when the pump and drive are power limited and the estimated design mixture velocity is close to the deposit limit velocity. Or for instance when a wide range of particle sizes is expected, where the average particle diameter will change in time, and as such u_{dl} fluctuates as a function of the particle size.

The new insights also put into perspective why long distance dredging pipelines are traditionally designed at concentrations below 0.15. Namely, if a sliding bed density wave forms, the peak could grow to twice the average concentration, thus 0.30. This is still on the safe side. If for instance the pipeline average concentration is designed at 0.20, and the mixture velocity drops below the deposit limit velocity for a short period, a density wave forms with a peak concentration of 0.4. This concentration is high enough that inter-particle and particle–wall forces start dominating frictional losses, and basically the wave becomes a mobile sediment plug (van den Berg, 2013). The plug has high resistance with the pipe wall (Visintainer et al., 2023), slowing down the mixture in the pipe, and leading to a pipeline blockage if the wave is long enough.

Erosion driven density waves form less risk to long pipelines that operate close to the deposit limit velocity. The argument is twofold. Firstly, if density waves are formed, their amplitude will grow to $c_{w,peak} = 1.5c_{w,mean}$, which is less than sliding bed waves. This also suggests that long pipelines transporting fine sand can be designed for slightly higher concentrations, perhaps to an average concentration of 0.2 (then waves will grow to 0.30, which is still considered safe). Secondly, the erosion driven density waves need more time develop to full amplitude, compared to the sliding bed driven density waves. Therefore, if the pipeline mixture velocity drops below u_{dl} for a short period, the wave might not have the time to fully develop and become large enough to impede the safety of the pipeline. In contrary, the sliding bed driven density waves develop very quickly, and could grow to full amplitude if the mixture velocity temporarily drops below u_{dl} for a short period. Exactly how short this period may be, is still difficult to estimate with the current knowledge.

One question remains: What density wave mechanism was predominating the Prins Clausplein pipeline? The arguments for sliding bed driven waves are: (i) The wave peaks are ∼2.0 times the mean concentration. (ii) The wave celerity in the Prins Clausplein case was observed to be able to exceed the mixture velocity (Matoušek, 1996). This is also the case of the sliding bed driven density observed in this research and in the research of Matoušek and Krupička (2013). The arguments for erosion driven waves are: (i) the mean particle diameter in the Prins Clausplein pipeline is in the range of 100–300 μm, and from the experiments of this research that would indicate erosion driven waves. (ii) The growth rate of the Prins Clausplein pipeline seems low, requiring tens of minutes to develop, and do not seem to grow almost instantly as seen in the sliding bed driven waves of this experiment. This last argument however is not that solid, since it is not known how much time the Prins Clausplein pipeline actually operated below u_{dl}. If the pipeline would have constantly operated below u_{dl} then sliding bed driven waves would formed rapidly, based on lessons learnt in this research. However, if the pipeline only sporadically operated below u_{dl} than even the growth rate of sliding bed density waves would seem low.

A strong counter argument against sliding bed driven waves in the Prins Clausplein pipeline is the particle size, being similar to particle sizes that showed erosion driven waves in this research. However, it was reported that the distribution of particle was very broad with 0.07 by volume larger than 700 μm, which is large enough to cause sliding bed driven waves. The experiments of this research were well graded sands, thus a direct comparison of mean particles sizes might not be valid. If sliding bed driven density waves were indeed the main mechanism in the Prins Clausplein pipeline, then the waves were caused by the larger fractions of the particle size distribution. Whether this is possible is a important research question for future research, since broadly graded sediments are very common in practical applications.

5. Conclusions

This research was dedicated to study the effect of the particle diameter and concentration on the formation of self-amplifying density waves in horizontal hydraulic transport pipeline. The experiments revealed that Talmon et al. (2007) and Matoušek and Krupička (2013) were studying two different density wave mechanisms in hindsight. The experiments of this research clearly distinguish the two wave types.

Erosion driven density waves are caused by the erosion-sedimentation imbalance (Talmon, 1999). Erosion driven density waves developed in case of finer sands, in this research 242 and 308 μm. Erosion driven density waves develop relatively slowly, and can reach a peak amplitude 1.5 times the average concentration of the mixture, as found in this research.

Sliding bed driven density waves, are caused by the inverse proportionality between the deposit limit velocity and the concentration, at mean mixture concentrations above ∼0.1. These waves form the highest risk for hydraulic transport pipelines compared to the erosion driven density waves, since the sliding bed driven density waves reach their peak amplitude very rapidly, and their amplitude can grow to twice the average mixture concentration, as found in this research.

The density wave data generated is very useful for future numerical modeling of these processes. First steps towards numerical modeling have already been made in de Hoog et al. (2024). Furthermore, the new knowledge already provides valuable insights for pipeline designers today. Long distance pipelines are always designed conservatively with concentrations not exceeding ∼0.15. The new insights in the mechanisms responsibly for density waves, explains how this conservative limit came to be. In addition, we know that erosion driven density waves are not as risky as sliding bed driven density waves, therefore the design limit can be chosen less conservatively. An open question remains: What is the influence of the particle size distribution on the type of wave that develops? Can a broad distribution lead to sliding bed driven density waves, while the mean particle size is low (∼< 300 μm)? This question should be answered as part of future research.

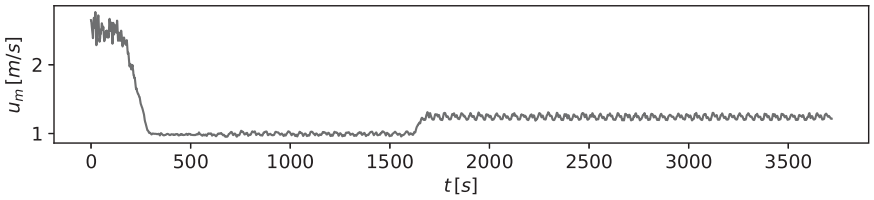

(a) Mixture velocity

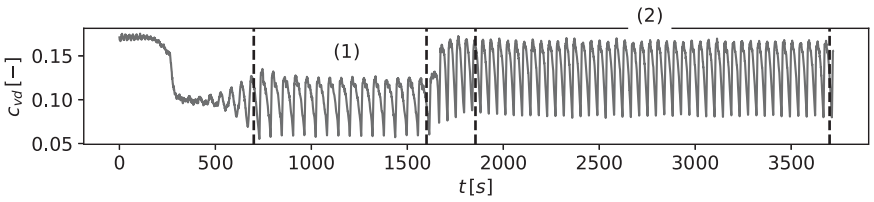

(b) Delivered concentration

Fig. 14. Tests Zilverzand (Zz), nrs. 2.1 and 2.2, $d_{50} = 242$ µm.

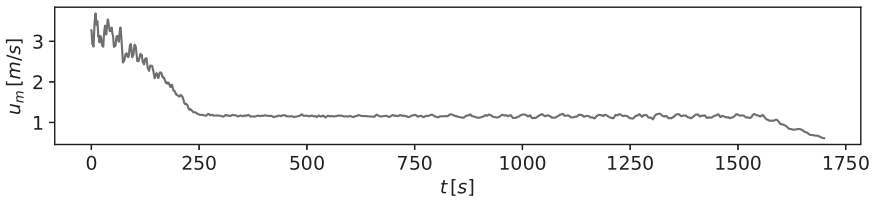

(a) Mixture velocity

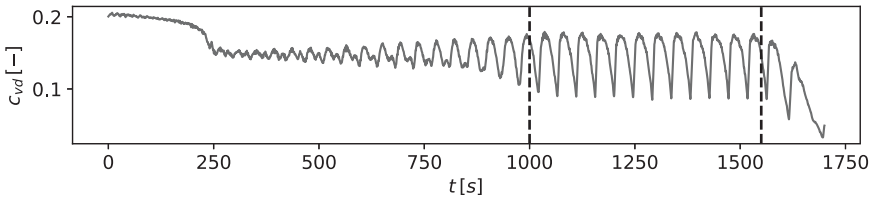

(b) Delivered concentration

Fig. 15. Tests Zilverzand (Zz), nrs. 3.1 and 3.2, $d_{50} = 242$ µm.

CRediT authorship contribution statement

Edwin de Hoog: Conceptualization, Formal analysis, Investigation, Methodology, Resources, Validation, Writing – original draft. **Oscar van der Ven:** Conceptualization, Formal analysis, Investigation, Methodology, Data curation. **Rudy Helmons:** Resources, Supervision, Writing – review & editing. **Arno Talmon:** Methodology, Supervision, Writing – review & editing. **Cees van Rhee:** Project administration, Resources, Supervision.

Declaration of competing interest

The authors declare the following financial interests/personal relationships which may be considered as potential competing interests: Edwin de Hoog reports financial support was provided by Royal IHC. Cees van Rhee reports financial support was provided by TKI Maritiem. Edwin de Hoog reports a relationship with Royal IHC that includes: employment. If there are other authors, they declare that they have no known competing financial interests or personal relationships that could have appeared to influence the work reported in this paper.

Acknowledgments

This research was funded by Royal IHC and TKI Maritiem. We would like to thank Yarno Ketting for his help in the construction and design of the experimental setup. We thank Václav Matoušek for the idea that the reduced cross-section above the bed layer could increase the wave celerity. A special thanks has to go to Cees van Rhee, full Professor in Dredging Engineering. As a pioneer he introduced us into the exciting topic of dredging engineering and deep sea mining. Cees unexpectedly passed away at the age of 64. We will remember him as a dear colleague and an inspiring mentor.

Appendix. Figures of all experiments

See Figs. 14–26.

Data availability

Data will be made available on request.

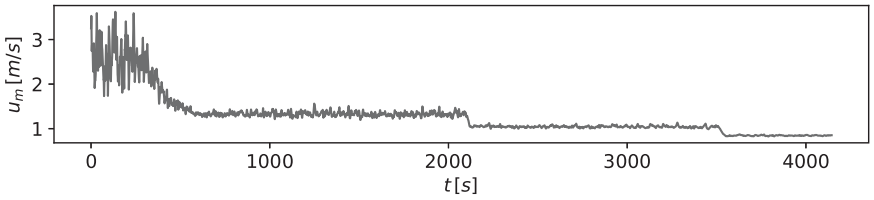

(a) Mixture velocity

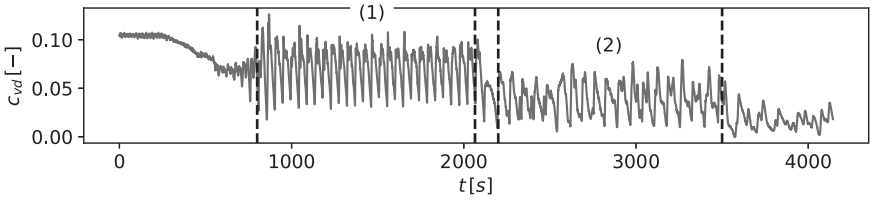

(b) Delivered concentration

Fig. 16. Tests Dorsilit 9 (D9), nrs. 1.1 and 1.2, $d_{50} = 308$ µm.

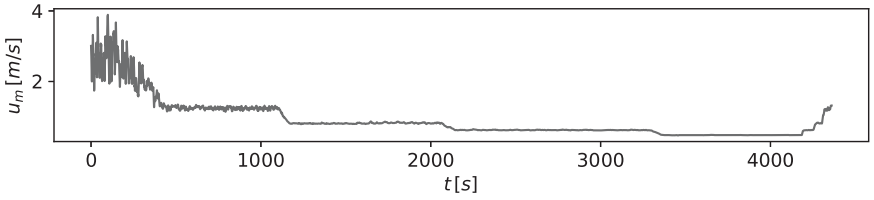

(a) Mixture velocity

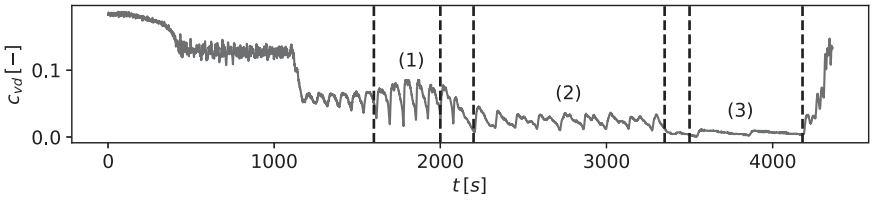

(b) Delivered concentration

Fig. 17. Tests Dorsilit 9 (D9), nrs. 2.1, 2.2 and 2.3, $d_{50} = 308$ µm.

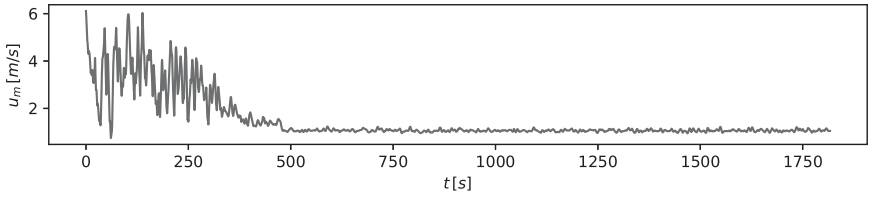

(a) Mixture velocity

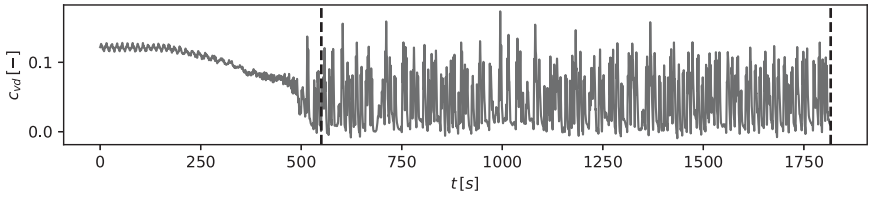

(b) Delivered concentration

Fig. 18. Tests Dorsilit 8 (D8), nr. 1, $d_{50} = 617$ µm.

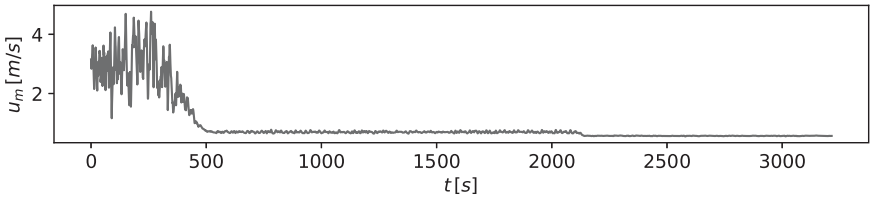

(a) Mixture velocity

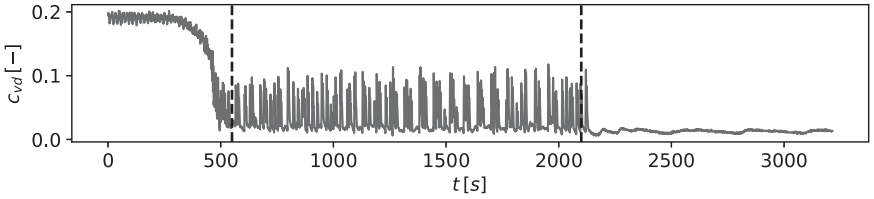

(b) Delivered concentration

Fig. 19. Tests Dorsilit 8 (D8), nr. 2, $d_{50} = 617$ µm.

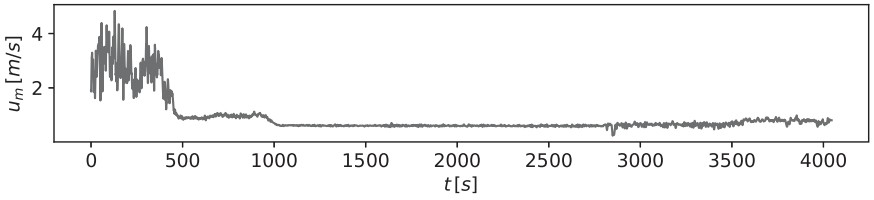

(a) Mixture velocity

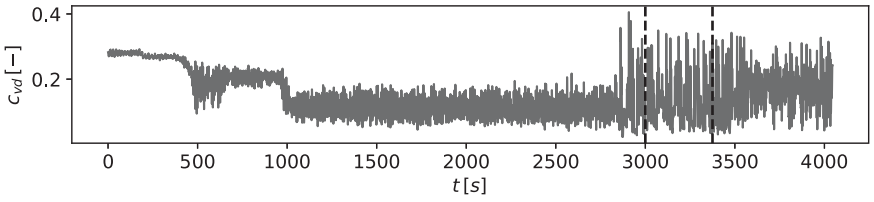

(b) Delivered concentration

Fig. 20. Tests Dorsilit 8 (D8), nr. 3, $d_{50} = 617$ µm.

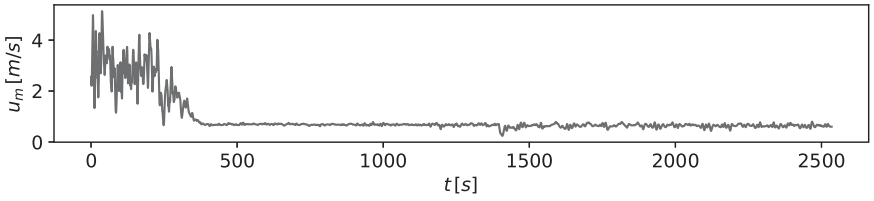

(a) Mixture velocity

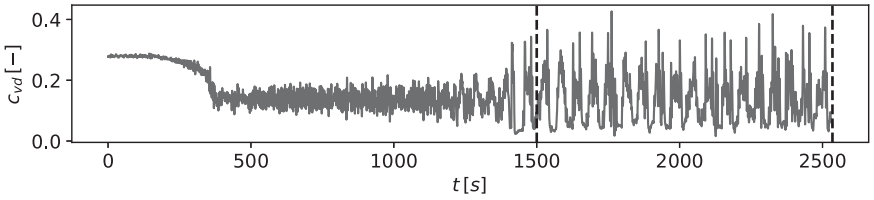

(b) Delivered concentration

Fig. 21. Tests Dorsilit 8 (D8), nr. 4, $d_{50} = 617$ µm.

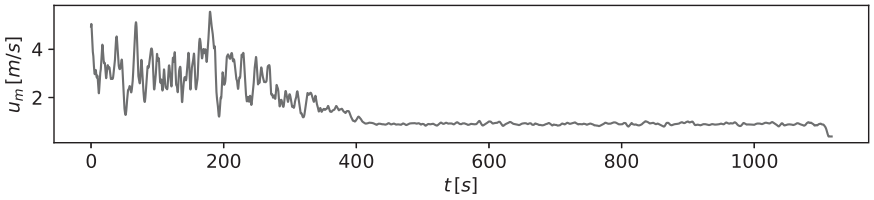

(a) Mixture velocity

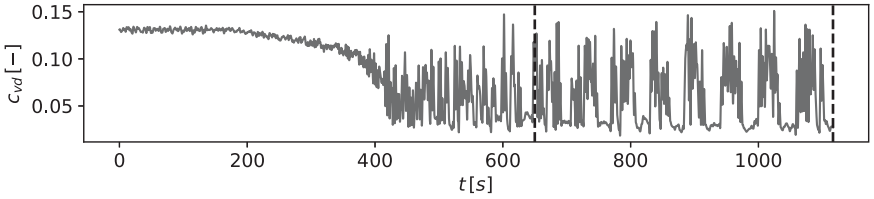

(b) Delivered concentration

Fig. 22. Tests Dorsilit 7 (D7), nr. 1, $d_{50} = 1.08$ mm.

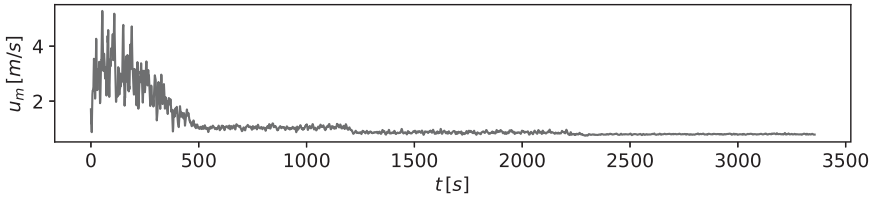

(a) Mixture velocity

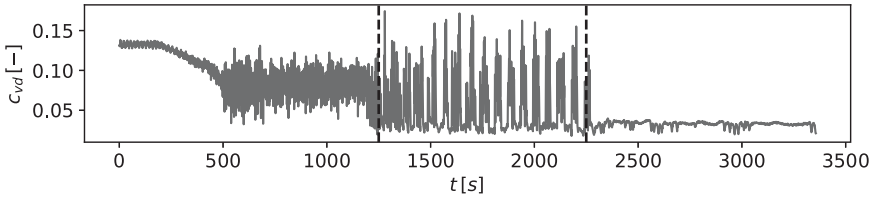

(b) Delivered concentration

Fig. 23. Tests Dorsilit 7 (D7), nr. 2, $d_{50} = 1.08$ mm.

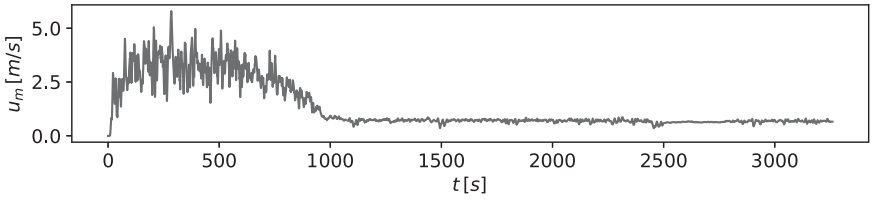

(a) Mixture velocity

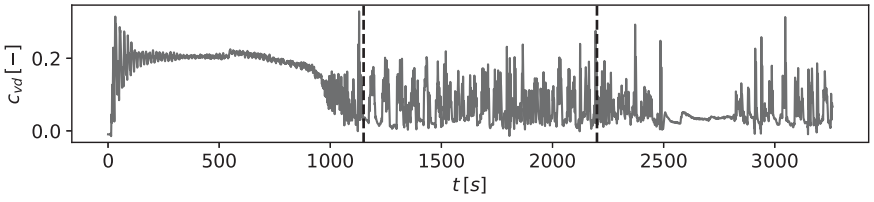

(b) Delivered concentration

Fig. 24. Tests Dorsilit 7 (D7), nr. 3, $d_{50} = 1.08$ mm.

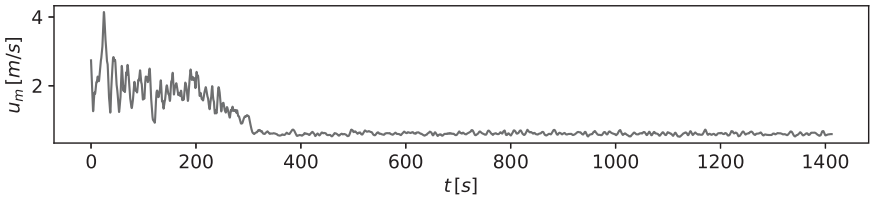

(a) Mixture velocity

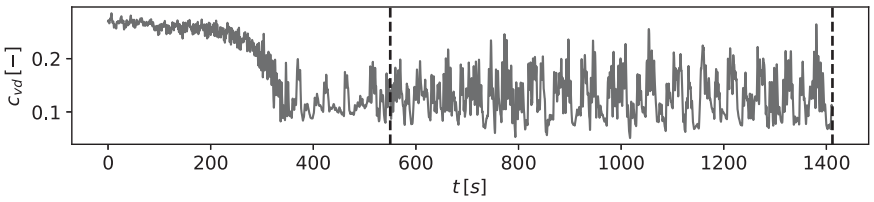

(b) Delivered concentration

Fig. 25. Tests Dorsilit 7 (D7), nr. 4, $d_{50} = 1.08$ mm.

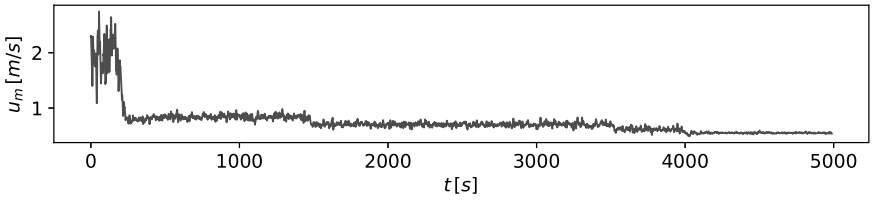

(a) Mixture velocity

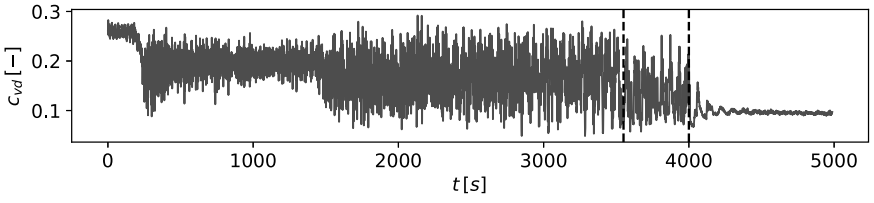

(b) Delivered concentration

Fig. 26. Tests Dorsilit 7 (D7), nr. 5, $d_{50} = 1.08$ mm.

References

Bisschop, F., 2018. Erosion of Sand at High flow velocities: An experimental study (Ph.D. thesis). Delft University of Technology.

Clift, R., Clift, D.H., 1981. Continuous measurement of the density of flowing slurries. Int. J. Multiph. Flow 7 (5), 555–561.

de Hoog, E., Talmon, A.M., van Rhee, C., 2021. Unstable transients affecting flow assurance during hydraulic transportation of granular two-phase slurries. J. Hydraul. Eng. 147 (9), 04021029.

de Hoog, E., van der Voort, T., Talmon, A.M., van Rhee, C., 2024. A 1-dimensional-two-layer transient drift-flux model for hydraulic transport pipelines: modeling and experiments of bed layer erosion and density wave amplification. J. Hydrol. Hydromech. 72 (1).

de Hoog, E., van Wijk, J.M., Talmon, A.M., van Rhee, C., 2022. Predicting density wave amplification of settling slurries using a 1D Driftux model. Powder Technol. 400 (3), 117252.

Keetels, G.H., Chauchat, J., Breugem, W., 2023. Role of turbulent kinetic energy modulation by particle–fluid interaction in sediment pick-up. J. Fluid Mech. 955, F02003.

Matoušek, V., 1996. Solids transportation in a long pipeline connected with a dredge. Terra Aqua 62 (1), 3–11.

Matoušek, V., Krupička, J., 2013. Different types of unsteady flow of solids generated in laboratory slurry pipe loop. In: 16th Conference on the Transport and Sedimentation of Solid Particles.

Matoušek, V., Krupička, J., Kesely, M., 2018. A layered model for inclined pipe flow of settling slurry. Powder Technol. 333, 317–326.

Richardson, J.F., Zaki, W.N., 1954. Sedimentation and fluidisation: Part I. Trans. Inst. Chem. Eng. 32, pp. 35.

Talmon, A.M., 1999. Mathematical analysis of the amplification of density variations in long-distance sand transport pipelines. In: 14th International Conference on Slurry Handling and Pipeline Transport. Maastricht, the Netherlands, pp. 3–20.

Talmon, A.M., Aanen, L., Bakker-Vos, R., 2007. Laboratory tests on self-excitation of concentration fluctuations in slurry pipelines. J. Hydraul. Res. 45 (5), 653–660.

Taylor, G.I., 1954. The dispersion of matter in turbulent flow through a pipe. Proc. R. Soc. Lond. Ser. A Math. Phys. Sci. 223 (1155), 446–468.

van den Berg, C.H., 2013. IHC Handbook for Centrifugal Pumps and Slurry Transportation, first ed. MTI Holland B.V., Kinderdijk, the Netherlands.

van Rhee, C., 2010. Sediment entrainment at high flow velocity. J. Hydraul. Eng. 136, 572–582.

van Rijn, L.C., 1984. Sediment pick–up functions. J. Hydraul. Eng. 110 (10), 1494–1502.

Visintainer, R., Matoušek, V., Pullum, L., Sellgren, A. (Eds.), 2023. Slurry Transport Using Centrifugal Pumps. Springer International Publishing, Cham.

Wilson, K.C., Addie, G.R., Sellgren, A., Clift, R., 2006. Slurry Transport using Centrifugal Pumps, third ed. Springer US.

Winterwerp, J.C., Groot, M.B.d., Mastbergen, D.R., Verwoert, H., 1990. Hyperconcentrated sand–water mixture flows over a flat bed. J. Hydraul. Eng. 116 (1), 36–54.